ORIGINAL ARTICLE

Society For Biomaterials | **WILEY**

Decellularized grass as a sustainable scaffold for skeletal muscle tissue engineering

Scott J. Allan[1,2] | Marianne J. Ellis[2] | Paul A. De Bank[3]

[1]EPSRC Centre for Doctoral Training, Centre for Sustainable Chemical Technologies, University of Bath, Bath, UK

[2]Department of Chemical Engineering, University of Bath, Bath, UK

[3]Department of Pharmacy & Pharmacology and Centre for Therapeutic Innovation, University of Bath, Bath, UK

Correspondence

Dr Paul A. De Bank, Department of Pharmacy & Pharmacology, Centre for Therapeutic Innovation, University of Bath, Bath, BA2 7AY, UK.
Email: p.debank@bath.ac.uk

Abstract

Scaffold materials suitable for the scale-up and subsequent commercialization of tissue engineered products should ideally be cost effective and accessible. For the *in vitro* culture of certain adherent cells, synthetic fabrication techniques are often employed to produce micro- or nano-patterned substrates to influence cell attachment, morphology, and alignment via the mechanism of contact guidance. Here we present a natural scaffold, in the form of decellularized amenity grass, which retains its natural striated topography and supports the attachment, proliferation, alignment and differentiation of murine C2C12 myoblasts, without the need for additional functionalization. This presents an inexpensive, sustainable scaffold material and structure for tissue engineering applications capable of influencing cell alignment, a desired property for the culture of skeletal muscle and other anisotropic tissues.

KEYWORDS

cultured meat, decellularization, scaffold, skeletal muscle, tissue engineering

1 | INTRODUCTION

The use of cytocompatible substrate materials as scaffolds for *in vitro* culture of adherent cells is commonplace within toxicology, tissue engineering, regenerative medicine and the emergent fields of cell-based therapeutics and cultured meat. Biomaterials include polymers (synthetic and natural), ceramics, metals and metal composites with many natural polymers of animal origin, such as collagen and gelatin, subject to environmental and ethical concerns and batch-to-batch variation.[1-3] Many of these materials, especially synthetic polymers, may require functionalization or chemical modification to support cell attachment, and suitable materials are typically chosen based on the following characteristics: biocompatibility, biodegradability, mechanical properties, scaffold architecture/form and manufacturing technology requirements.[1] Tissue engineering scaffolds can be fabricated in various morphologies including, but not limited to, 2D films, 3D sponges, microparticles, fibres and hydrogels. These are generated from materials in starting-forms including liquid solutions, powders, and gels, with a processing step from feedstock material to a scaffold-suitable structure. An alternative to this is to dissociate and remove the cellular components of tissues or organs, leaving behind the extracellular matrix (ECM) as a ready-formed 3D scaffold, sometimes referred to as a "ghost organ". This approach has been demonstrated with both animal and plant tissues and methods of decellularization are typically chemical and/or enzymatic (e.g., surfactants, acids and bases and trypsin) or mechanical (e.g., freeze–thaw, agitation, sonication, supercritical CO_2, hydrostatic pressure).[4-6] The natural backbone material of the remaining ECM differs depending on the source; largely collagen, laminin and fibronectin from animal-derived tissues[4,7] and a primarily cellulose backbone with varying proportions of pectin and hemicellulose from plant-derived structures.[8-10] Multiple reviews exist on the use of decellularized animal tissues and organs as biomaterials for tissue engineering (intended for *in vivo* implantation) and examples include decellularized hearts and heart valves, skin, small intestine, liver, kidney, cornea, blood vessels, lung, myocardium and cell sheets.[4,5,11,12]

For applications in regenerative medicine, the use of animal tissue presents the advantage of structural similarity and even like-for-like organs, but the main disadvantage is that they still require donor tissues or organs, introducing ethical and/or availability concerns. The abundance of plants in nature means their decellularized ready-formed structures present a sustainable, ethical and inexpensive input alternative. Plant tissues that have been decellularized by detergent treatment and re-seeded with mammalian cells include apple slices, spinach leaves, bamboo, orchid, vanilla, *anthurium magnificum* and *anthurium warocqueanum*, parsley, *calathea zebrina*, wasabi, green onion, celery, carrot, broccoli, sweet pepper, persimmon and jujube.[8,9,13–17] The cell wall in plants, as a type of ECM, remains intact and is primarily cellulose, which is the most abundant organic polymer on earth[18] and has been shown to be cytocompatible in various studies.[8,9,13,19–23]

Tissue engineering of skeletal muscle has been reviewed for potential applications in regenerative medicine, tissue replacement, cell-based therapies, drug testing and toxicology screening, and for consumption in the form of cultured meat, also known as *in vitro* and cell-based meat.[3,24–28] The final form and functionality of the engineered tissue will differ depending on the intended application, however engineering skeletal muscle *in vitro* with the intent of achieving functional muscle requires uniaxial alignment of muscle fibres due to the directional-dependent, anisotropic characteristic and structure of muscle. Studies have shown that alignment of myoblasts prior to differentiation enables aligned myotubes to be engineered.[29,30] Methods of such alignment include active stimulation (electrical or mechanical) or passive methods such as modifying substrate mechanical properties, for example, stiffness, or surface morphology to introduce topographic cues that promote cell alignment via contact guidance.[23,31–38]

Grass as a proposed scaffold material meets the criteria of being readily available due to its abundance in nature and it was hypothesized that the long narrow leaves and parallel vasculature system in grass blades, a characteristic of monocot plant leaves, may support the self-alignment of cells following seeding. Hence, the aim of this study was to investigate the novel prospect of using decellularized grass as a scaffold for the *in vitro* culture of myoblasts. Here we report the decellularization of amenity grass, the characterization of its topography and its cytocompatibility with murine myoblasts in terms of attachment, viability, proliferation, and differentiation. Overall, this study demonstrates the suitability of decellularized grass as a scaffold for the tissue engineering of aligned myofibres via the passive mechanism of contact guidance.

2 | MATERIALS AND METHODS

2.1 | Grass decellularization

Grass blades were obtained from the University of Bath grounds. This is amenity grass suspected to be a combination of rye grass, fescue grass, and/or annual bluegrass. Blades were pre-treated by washing for 5 min with ethanol (VWR Chemicals, 20821) followed by 5 min with phosphate-buffered saline (PBS; Sigma-Aldrich, D8537). This sequential washing was repeated a further two times. Grass blades were then soaked and agitated in 1% (w/v) sodium dodecyl sulphate (SDS; Sigma-Aldrich, L4509), 1% (v/v) Tween-20 (Sigma-Aldrich, P1379), and 10% (v/v) bleach (The Consortium, 049403) at 150 ml decellularization working solution per gram of grass for 1 to 2 days until all blades were visually translucent. Following decellularization, grass blades were washed with MilliQ water and stored in PBS at 4°C prior to use.

2.2 | Measurement of grass blade thickness

The thickness of native and decellularized grass was measured using an electronic micrometer (RS Pro External Micrometer, 705–1,229, range 0–25 mm, resolution 0.001 mm). Data are expressed as the mean ± SD of the reported sample size of n individual grass blades using the average of two readings at different points along the length of each blade. Measurements were conducted on grass blades air dried for >3 hr at room temperature. Native grass was cut fresh prior to drying out. Decellularized grass was removed from 4°C PBS prior to drying.

2.3 | Scanning electron microscopy

Grass blades, either pre- or post-decellularization, were frozen at −80°C for 3 hr and lyophilized overnight using a Thermo Savant MicroModulyo-230 freeze dryer. Samples were then coated with a 50 nm layer of gold in an Edwards Sputter Coater S150B and imaged on a JEOL JSM-6480LV SEM.

2.4 | Atomic force microscopy

Atomic force microscopy (AFM) was utilized to determine the topography of lyophilized samples of decellularized grass in ambient air. AFM experiments were performed in tapping mode on a Bruker Multimode Nanoscope IIIA AFM machine with a NuNano Scout 70 silicon probe (spring constant of 2 N/m and resonant frequency of 70 kHz). Gwyddion software was used to analyse the AFM images and generate the overlay 3D images of the topography.

2.5 | Profilometry

A Proscan 2000 non-contact surface profilometer with a chromatic sensor (sensor type S5/03) at a sample rate of 300 Hz and 200 steps (step size of 2 μm) was used to characterize the surface morphology of lyophilized samples of decellularized grass in ambient air, in the micrometre range.

2.6 | Cell culture

The murine myoblast cell line C2C12 (ECACC 91031101) was used to model skeletal muscle cells. Cells were maintained in proliferation medium consisting of high glucose Dulbecco's Modified Eagle's Medium (DMEM; Sigma-Aldrich D5796) supplemented with 10% (v/v) foetal bovine serum (FBS; Gibco™, Thermo Fisher Scientific 10270106) and 1% (v/v) penicillin/streptomycin (P/S; Sigma-Aldrich P4333) in a humidified incubator at 37°C and 5% CO_2. Cells were maintained in T-75 culture flasks and passaged approximately every 3 days until reaching ~80% confluence, at which point they were sub-cultured.

2.7 | Cell adhesion on decellularized grass

Prior to cell seeding, grass blades were sterilized by soaking in 70% (v/v) ethanol (VWR Chemicals, 20821) for 1 hr, followed by washing in proliferation medium and pre-treatment by soaking in proliferation medium overnight at 4°C. Attachment of C2C12 cells to native grass (i.e., blades incubated in 70% ethanol for 1 hr but, otherwise, untreated) or decellularized grass was then assessed by seeding a 1 cm long section of an untethered grass blade with 5,000 cells cm^{-2}, relative to the surface area of a well, in a 24-well cell culture plate. Cells were seeded by pipetting 0.5 ml of cell suspension into a well which contained an untethered, sterile grass blade on its surface. Following a 3 hr attachment period, blades were incubated with the live cell stain fluorescein diacetate (FDA; Acros Organics 191660050) for 5 min at room temperature and nuclei were counterstained with Hoechst 33342 (ThermoFisher Scientific, H21492; 1:2,000 dilution of Hoechst stock solution [10 mg/ml in deionized water] in PBS) for 10 min at room temperature. Samples were washed once with PBS and imaged in DMEM without FBS using a Leica inverted microscope (Leica DMI4000B). FDA staining solution was prepared as 1.6 μl/ml FDA solution in DMEM without FBS from a stock solution of 5 mg/ml FDA in acetone. The cell attachment per cm^2 of grass blade was quantified by nuclei counting using the cell counter feature of the image analysis software suite, Fiji (a distribution of ImageJ).[39]

2.8 | Assessment of cell proliferation and viability on decellularized grass

Proliferation and viability of C2C12 cells on decellularized grass was assessed by seeding decellularized grass blades as described above in a low-attachment 24-well plate (Fisher, 10327701). Live cells were stained with FDA on days 1, 3, and 6 post-seeding and nuclei were counterstained with Hoechst as described above before fluorescence imaging to determine the number of live cells at each time point. Viability of C2C12 cells was determined at 7 days post-seeding by staining with a live/dead stain of FDA as described above and propidium iodide (PI; Fisher, 11425392; 1:100 dilution in DMEM without FBS, of a 2 mg/ml PI stock solution in PBS).

2.9 | Differentiation of myoblasts on decellularized grass

Differentiation of C2C12 cells on decellularized grass was assessed by seeding 1 cm long sections of untethered grass blades with 50,000 cells cm^{-2}, relative to the surface area of a well, in a low-attachment 24-well plate. Cells were cultured in proliferation medium for 2 days and then differentiation medium for 7 days. Differentiation medium consisted of high glucose DMEM supplemented with 2% (v/v) horse serum (Sigma-Aldrich, H1270) and 1% (v/v) P/S. Samples were then stained using FDA and Hoechst and imaged with a Leica DMI4000B microscope as described above.

2.10 | Directionality and cell orientation analysis

Cell alignment on decellularized grass and tissue culture plastic was assessed using $10\times$ magnification images obtained from the proliferation assay described above. Fluorescent images of C2C12 cells stained with FDA on decellularized grass were compared with brightfield images of C2C12 cells in multiwell tissue culture plastic plates, both seeded at 5,000 cells cm^{-2} based on the surface area of a well. Images were converted to 8-bit and cropped to the in-focus portion of the image for the grass blades. The angle of the grass blade was measured using the ImageJ line measurement tool and the image then rotated with a reference point of 0° in the East direction (degree of rotation differed per image based on the angle of grass in the raw image, with images rotated so that grass blades were horizontal). Cell alignment was quantified using the *Directionality* plug-in of the image analysis software suite, Fiji (a distribution of ImageJ)[39] with the Fourier components method (number of bins = 90, between −90° and 90°). The same method was used to quantify the alignment of multinuclear myotubes.

Cell alignment on decellularized grass was also assessed based on orientation of nuclei using the image processing software, CellProfiler™.[40] A pipeline was developed to identify and measure the orientation of Hoechst-stained nuclei in $20\times$ magnification images from the proliferation assay as described above. Nuclei were identified in grey-scale images using the *IdentifyPrimaryObjects* module, with the following advanced settings: 40 to 100 pixel object diameter, *Adaptive* threshold strategy using the Otsu method with two classes and an adaptive window size of 200, and 1.3488 threshold smoothing scale. Clumped objects were distinguished by the *Intensity* method and separated with dividing lines based on *Shape*. Orientation was determined using the *MeasureObjectSizeShape* module. The distribution of the orientation of C2C12 cells on decellularized grass was used as a measure of alignment by expressing the orientation, θ (°), of the elongated cells relative to the direction of the grass blade channels, i.e. percentage of cells with orientation, θ within x° of the grass blade axis.

2.11 | Statistical analysis

Captions for figures and tables describing experimental results state the number of experimental repeats (*n*), replicates (*N*) and error. Results are presented as mean ± standard deviation (SD) unless otherwise stated. A type two (unpaired) two-tailed *t* test, using the Analysis ToolPak add-in for Microsoft Excel, was used to assess significant differences between groups, comparing means of independent biological replicates unless otherwise stated. A value of p < 0.05 was considered statistically significant.

3 | RESULTS

3.1 | Decellularization of grass

The applicability of decellularized grass as a scaffold for the culture of mammalian cells required confirmation that the decellularization process employed was sufficient to remove the native plant cells and genetic material, while maintaining the ECM structure, to prevent cytocompatibility issues *in vitro* and potential adverse host response *in vivo*.[11] To this end, the degree of grass decellularization was
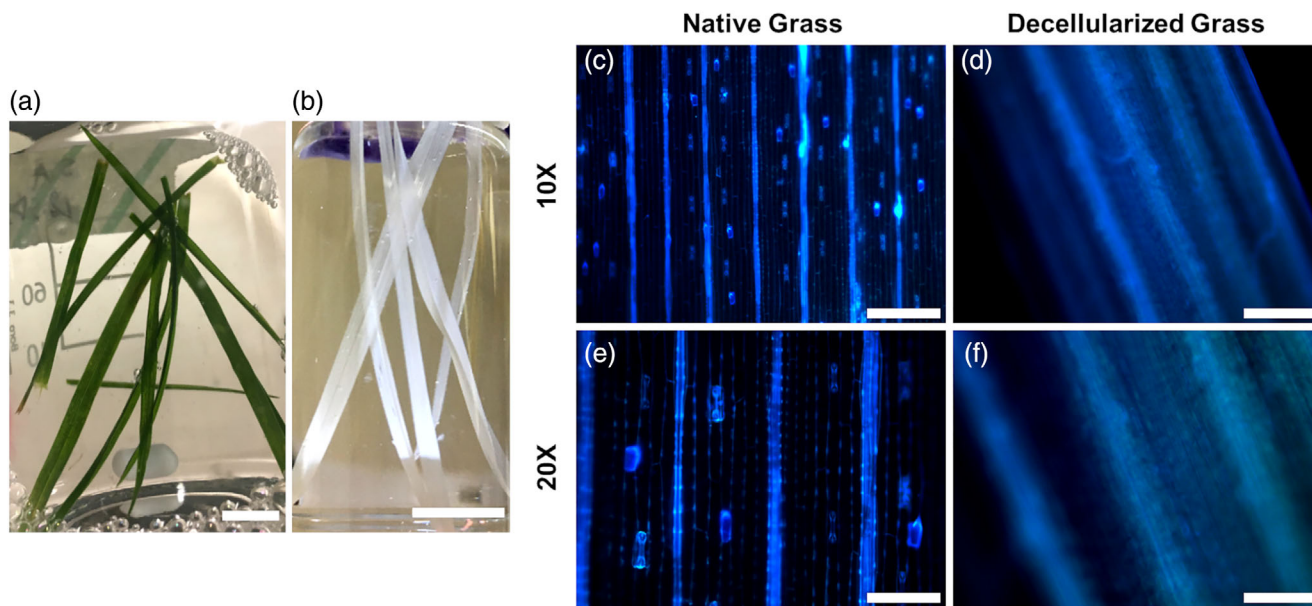

FIGURE 1 (a,b) Images of native grass (a) and decellularized grass (b). Scale bars: 1 cm. (c-f) Hoechst 33342 staining (blue) for nuclei in native grass (c,e) and decellularized grass (d,f). Scale bars: 200 μm (c,d) and 100 μm (e,f)
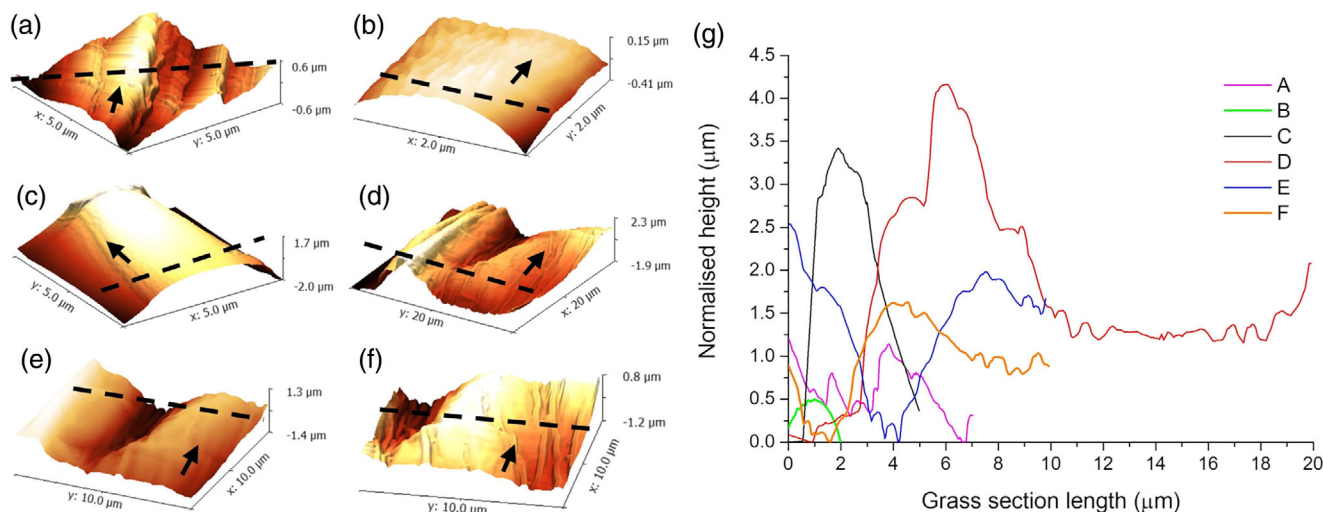

FIGURE 2 (a to f) 3D AFM images of decellularized grass and the corresponding topographic height plots (g) normalized to the minimum *z*-axis data point. Arrows = longitudinal direction of grass blade. Black dotted line = specific cross-section mapped onto the height plot

determined by visual inspection, using a colour and transparency sight-test (Figure 1(a,b)). When the grass blades had been stripped of all colour and become "ghost-like", decellularization was deemed complete. Following the decellularization process, the thickness of the grass blades decreased from 81 ± 11 μm ($n = 18$) for native grass to 75 ± 11 μm ($n = 18$) for decellularized blades (p > 0.05). Further qualitative confirmation of decellularization was conducted by Hoechst staining for nuclei, as one of the cell removal verification methods,[6] illustrating the absence of nuclei following the decellularization process (Figure 1(c-f)).

3.2 | Topography of decellularized grass

The hypothesized benefit of using grass as a plant-source scaffold is the anisotropic form of parallel vasculature presenting a natural surface pattern that may present cues for the passive alignment of cells. This presented the need to characterize the surface topography of grass to determine whether it was affected by the decellularization process. In addition to stripping grass blades of their cellular material, decellularization changed their surface roughness, as illustrated by the smoothing effect visible in SEM images (Figure S1). However, the backbone structure of grass was maintained as demonstrated by the AFM and profilometry scans of decellularized grass (Figure 2 and Figure 3).

These results confirm that the topography of decellularized grass is comprised of natural gratings/grooves giving rise to channels consisting of longitudinal, parallel striations, and demonstrate the scale of the z-direction height changes and feature size of the parallel striations visible using brightfield microscopy (Figure S2). The AFM images shown in Figure 2 illustrate the directional topography of decellularized grass. Due to the difference in mapping areas for images a-f from 2 × 2 μm up to 20 × 20 μm (x y), the height maps for a cross-section of each image have been plotted and normalized. This plot, Figure 2(g), shows that the directional, topographical features are present at both the nano-scale (<1 μm) and the lower end of the micro-scale (1 to 5 μm). Profilometry scans of decellularized grass (Figure 3) show that the parallel striations seen in light microscopy images (Figure S2) and SEM (Figure S1) are clearly distinguished as groove-like channels on the micro-scale, with a 400 × 400 μm (x y) mapping area illustrating height changes in the step-cliff features of $\Delta z \approx 0$ to 100 μm. From these data, it is apparent that, while the exact scales of these features vary slightly from blade to blade, aligned grooves are an inherent feature of grass and are retained in the decellularized scaffold.

3.3 | Cell attachment, proliferation and viability on decellularized grass

The use of a material as a cell scaffold is dependent on its cytocompatibility and consequent ability to support the attachment and proliferation of cells. With decellularized grass scaffolds in the context of this report, this represents the ability of the remaining plant ECM to support cell adhesion and growth. Without functionalization,
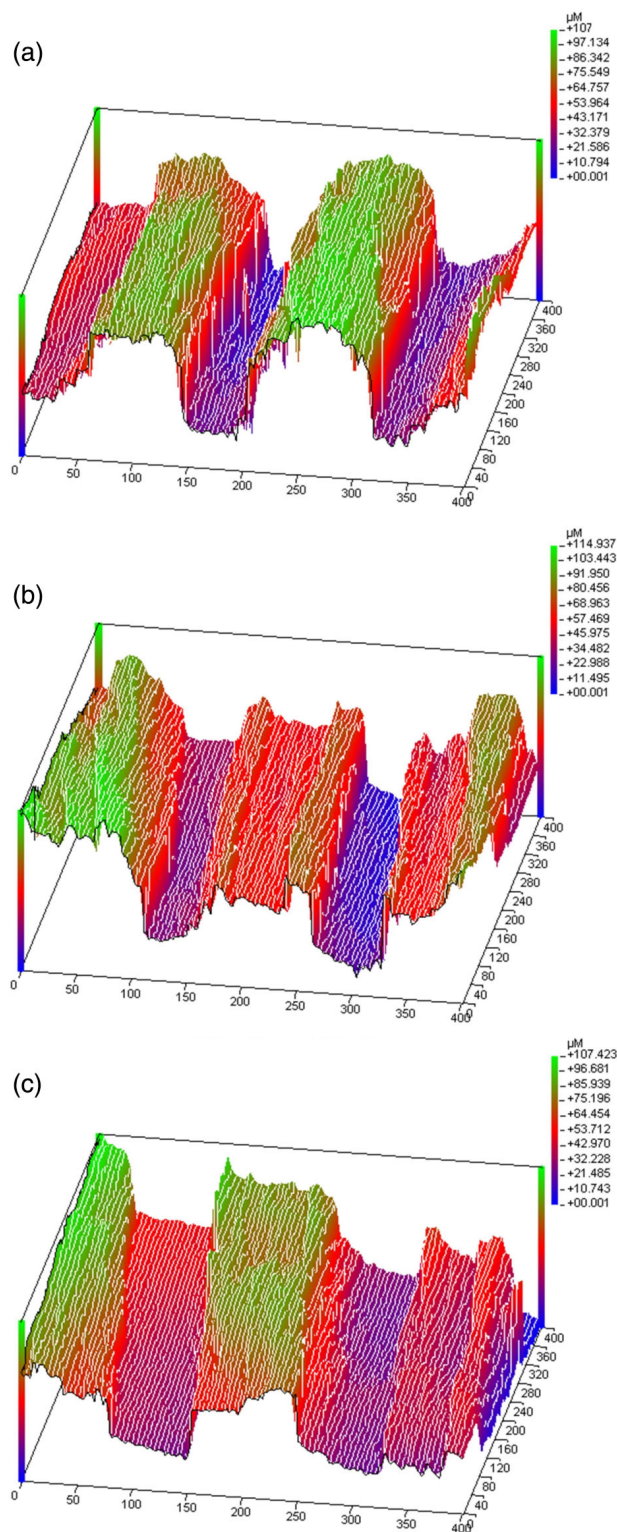

FIGURE 3 Decellularized grass blade surface morphology and topography visualized using a non-contact profilometer scan of a 400 × 400 μm mapping area

decellularized grass supported the attachment of C2C12 cells following a 3-hour attachment period with greater attachment efficiency than on native grass (Figure 4(a)). The attachment of C2C12 cells in
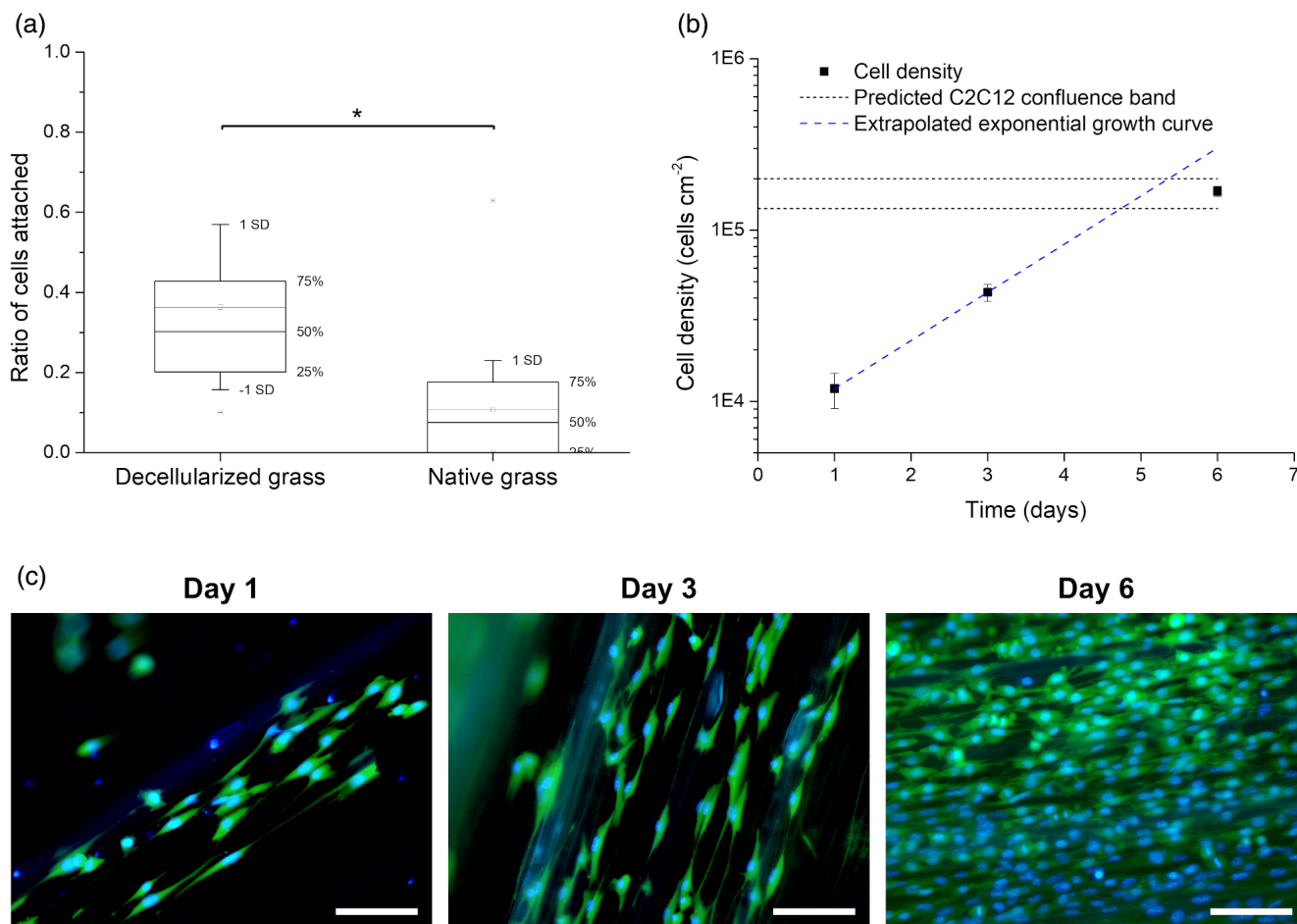
(a)

(b)

(c)

Day 1 **Day 3** **Day 6**

FIGURE 4 (a) Ratio of attached C2C12 cells on native and decellularized grass following a 3 hr attachment period. $n = 3$, attachment efficiency determined from greater than 15 images per sample type per repeat. Error bars (whiskers) = SD, mean presented by –o–. (b) Proliferation of C2C12 cells on decellularized grass. Data represents mean of $n = 3$, cell counts determined from 3 or more images per sample, error bars = SD. Exponential growth curve calculated based on doubling time between day 1 and 3 ($t_d = 25.7$ hr) and extrapolated (blue). Predicted lower and upper limit for C2C12 density at confluence presented (black). * indicates significance with $p < 0.05$. (c) Visual representation of C2C12 proliferation on decellularized grass over a 6 day period. Green = FDA stain for live cells. Blue = Hoechst 33342 stain for nuclei. Scale bars: 100 μm

this case was not comparable to tissue culture plastic (TCP), as the grass blades were not clamped or fixed to the bottom of the well. As a result, the percentage of cells contacting the available grass surface area was less than the number that would contact the plastic in a normal well. Figure 4(b) shows the growth curve for C2C12 cells on decellularized grass, with a calculated doubling time of 25.7 hr between day 1 and 3 post-seeding. This quantitatively demonstrates that cells reached confluence on the scaffold between 4 and 6 days post-seeding. Nuclei and live cell images from the proliferation assay on decellularized grass (Figure 4(c)) qualitatively show proliferation over a 6-day period of static culture and demonstrate self-alignment of the cells along the blades. Cells were observed to remain on the apical side of the grass blades, with no evidence of penetration into the scaffold. An overlay image of optical and fluorescence microscopy illustrates how alignment was parallel to the natural striations on grass blades (Figure S4). C2C12 cells on decellularized grass exhibited high levels of viability, with a live/dead assay on day 7 post-seeding

indicating that 95% of cells were viable (2 significant figures, $N = 3$; Figure 5).

3.4 | Quantification of cell alignment

To determine the effect of topographical cues presented by the natural surface topography of grass on cell behaviour, the orientation of C2C12 cells and their consequent alignment with the scaffold was characterized using the *Directionality* plugin of the image analysis software suite, ImageJ. A comparison was made between C2C12 myoblasts attached to decellularized grass and the accepted standard *in vitro* culture material of TCP (Figure 6). Representative microscopy images of C2C12 cells on TCP (Figure 6(a)) and decellularized grass (Figure 6(b) and S4) qualitatively demonstrate the distinction in orientation, with cells appearing to align with the grooves on the blades while exhibiting no noticeable alignment on

TCP. The relatively flat *Directionality* histograms obtained for cells attached to TCP (Figure 6(c)) indicates the isotropic nature of cell growth on this material, impl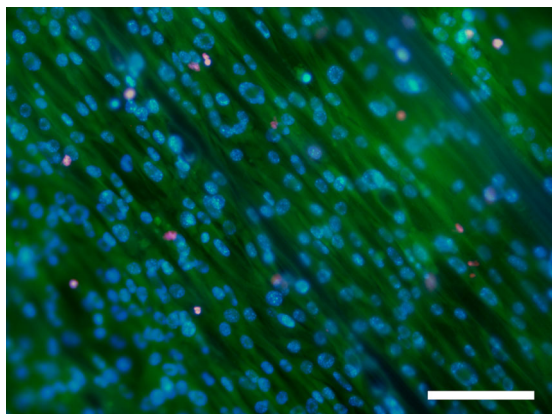ying it is random with no preferred orientation. By comparison, the histograms obtained for cells on decellularized grass have a clear peak for the preferred orientation, in the uniaxial direction parallel to the longitudinal natural striations present on the blades. This was quantified as 43% ± 8% ($\theta < \pm 10°$) and 59% ± 8% ($\theta < \pm 20°$), increasing up to 82% ± 5% ($\theta < \pm 50°$) from quantitation via the *Directionality* plug-in for ImageJ ($n = 3$, mean ± SD). While the percentage of cells with a preferred orientation on TCP of 14% ± 2% ($\theta < \pm 10°$) can be classified as random. Due to z-axis changes in height of the 3D grass blade, fluorescent micrographs were subject to areas in different focal planes and only in-focus sections were analysed for directionality and orientation to maximise accuracy. Further time course histograms (Figures S5 and S6) show that alignment or random orientation of myoblasts on grass and TCP, respectively, are not time-dependent, with C2C12 alignment seen as early as day 1 post-seeding on decellularized grass. To confirm the alignment of C2C12 cells, nuclear orientation based on the long-axes of nuclei was used as an indicator for cell alignment.[13,41] The image processing software CellProfiler™ was used to quantify nuclear orientation by first identifying the nuclei present (Figure 6(d,e)) and then measuring their orientation angle (Figure 6 (f)). This was quantified as 53% ± 4% ($\theta < \pm 10°$) and 72% ± 1% ($\theta < \pm 20°$) based on nuclear orientation ($n = 3$). The results obtained from this analysis indicated that a greater proportion of cells had a

FIGURE 5 Live/dead staining of C2C12 cells on decellularized grass scaffolds after a 7 day period of static culture. Merged fluorescence images of live stain (green) with FDA, dead stain (red) with PI, and nuclei stain (blue) with Hoechst 33342. Magenta indicates dead cells, where PI and Hoechst are co-localized. Scale bar: 100 μm
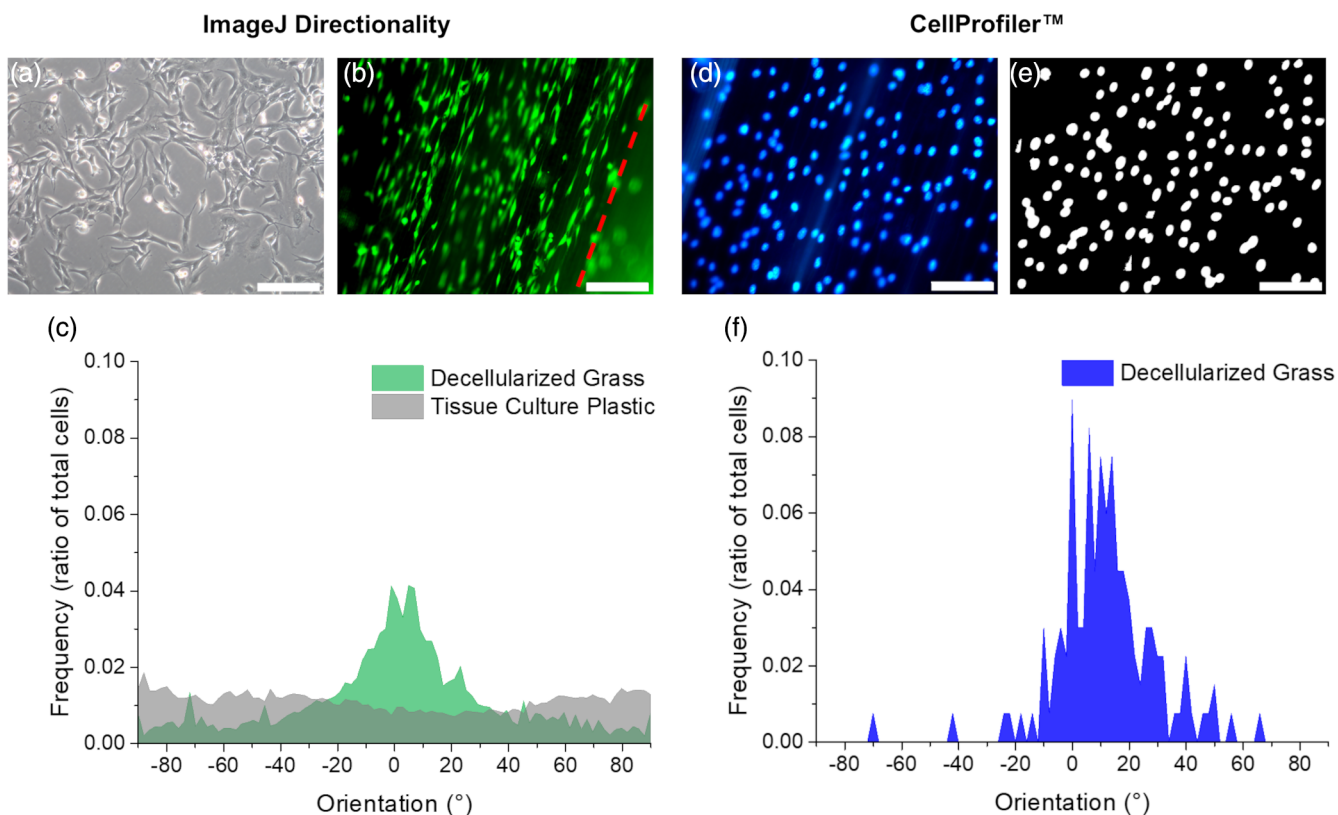

FIGURE 6 Directional orientation of C2C12 cells (day 3 post-seed) on (a) tissue culture plastic and (b) decellularized grass quantified in (c) histogram of cell orientation on day 3 of the proliferation assay, quantified using the ImageJ *Directionality* plug-in. (d) Nuclei of C2C12 cells on decellularized grass stained with Hoechst (e) nuclei identified and isolated using CellProfiler™ software (f) histogram of nuclei orientation quantified using CellProfiler™. Scale bars (a and b) 200 μm, (d) 100 μm. The red dashed line represents the right hand boundary of the region of image (b) analysed using the ImageJ *Directionality* plug-in
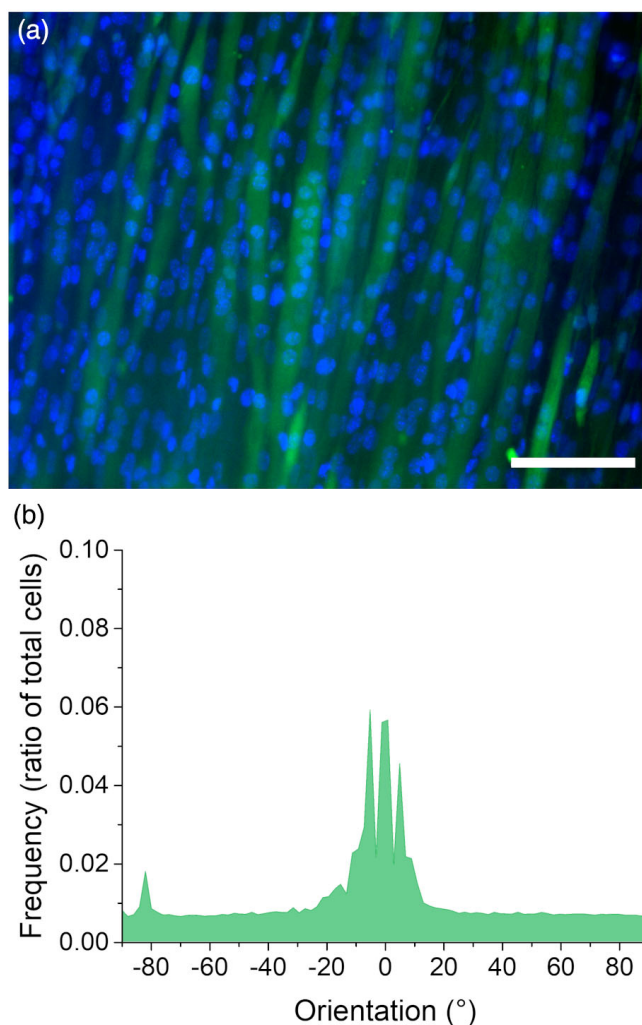
FIGURE 7 C2C12 myotubes on decellularized grass after 7 days in differentiation media. (a) Merged fluorescence images of C2C12 myotubes stained green with FDA and with nuclei stained blue with Hoechst 33342. (b) Frequency of aligned myotubes as a ratio of the total number of myotubes quantified using the ImageJ *Directionality* plug-in. Scale bar = 100 μm

preferred orientation parallel to the striations on the grass blade compared to the results quantified using the ImageJ *Directionality* plug-in.

3.5 | Myoblast differentiation on decellularized grass

A vital feature of a biomaterial scaffold for engineered skeletal muscle is its ability to support the differentiation of mononuclear cells such as myoblasts or satellite cells into myotubes, ideally in an aligned manner mimicking the anisotropic structure of natural muscle. Differentiation of C2C12 myoblasts on decellularized grass was confirmed following the culture of confluent cells in differentiation medium with a reduced serum content; Figure 7 clearly indicates the presence of aligned,

multinuclear myotubes on decellularized grass scaffolds. Alignment of myotubes was quantified using the ImageJ *Directionality* plug-in (Figure 7(b)).

4 | DISCUSSION

This article describes the use of decellularized grass scaffolds for the culture of C2C12 myoblasts, a model cell line for skeletal muscle tissue engineering applications. The detergent-based decellularization process was adapted from prior studies on plants[8,9,13] and is a simple procedure that can be performed in-house with the final-form scaffolds obtained in 1 to 2 days (Figure 1). With one of the potential applications of engineered muscle being for human consumption as cultured meat, our use of ethanol in the pre-treatment phase and Tween-20 as the non-ionic detergent, are favourable over the previously reported use of hexane and Triton X-100, respectively.[7,8,13] However, it is likely that traces of hexane and Triton X-100 would be removed following washing, sterilization and pre-treatment steps before cell seeding, as highlighted by Adamski, et al, through cell cytocompatibility studies.[42] Furthermore, for the application of edible scaffolds for cultured meat, it may not be sufficient for the substrate to be edible, non-toxic and texture-enhancing, but also nutritionally beneficial. In the case of decellularized grass, the complex cell walls of most grass species (save anomalies like maize) are not typically digestible without rumination. The composition of grass cell walls, as monocots, differ from most dicots, with greater proportions of hemicelluloses in both cell walls and lignin and silica in the secondary cell wall.[10] Consequently, further nutritional, compositional and bioavailability analysis should be conducted on decellularized grass preand post-cooking. In addition, the texture of food has a significant influence of consumer acceptance, and this will also require further investigation for the adoption of plant-based scaffolds in clean meat applications.

Decellularized grass as a naturally derived scaffold retains a topography comprised of parallel grating-like grooves. AFM and profilometry scans of decellularized blades (Figures 2 and 3), demonstrated that the surface topography of the grass blades consisted of longitudinal, parallel striations, in the uniaxial direction, a feature also visible using light microscopy (Figure S2). Topography analysis indicated the presence of grooves at both the nano- and micro-scale with variability resulting from the natural source (nano-scale in Figure 2 plots A, B and D to F (AFM), micro-scale in Figure 2 plot C to F (AFM) and Figure 3 (profilometry)). Due to limitations with AFM as a result of the tip crashing (mapping areas from 2×2 μm to 20×20 μm (x y) with height changes <5 μm), profilometry was used to further assess the topography of larger mapping areas (400×400 μm) and clearly demonstrated the presence of larger micro-scale features, with z-axis feature sizes (i.e., groove depths) up to ~100 μm (Figure 3). The area of decellularized blades scanned via AFM was, therefore, either on the top or bottom sections of the features visualized via profilometry. These grooves, although showing some variation in dimensions due to the natural source of the scaffold, are similar to those (sometimes

TABLE 1 Cell alignment on natural and synthetic topographic features. Unless otherwise specified, the cell type is C2C12 myoblasts

Substrate	Topography feature & size	OA ($\theta < x°$)	Alignment (%)	Alignment basis	Alignment quantitation method	Ref.
Natural topographic features of decellularized plants						
Grass	Channels <1 μm, 1–5 μm, and up to c.a. 100 μm	$\theta < 10°$ $\theta < 20°$	43 ± 8% 59 ± 8%	Myoblasts	ImageJ *Directionality*	This study
		$\theta < 10°$ $\theta < 20°$	53 ± 4% 72 ± 1%	Nuclei	CellProfiler™	
Solenostemon stems	Grooves [a]	$\theta < 20$	44 ± 7%	Nuclei (hDF)	CellProfiler™	[13]
Parsley stems		$\theta < 20$	29 ± 3%			
Green onion (i) Outer green leaf (ii) outer white bulb	Grooves W: (i) c.a. 9 (ii) 20–30 μm D: (i) 10–15 (ii) < 10 μm	- [b]	OOP 0.8–0.9	Actin filaments	2D orientation order parameter (OOP)	[14]
Synthetic topographic features						
TCP	Smooth	$\theta < 10°$	14 ± 2%	Myoblasts	ImageJ *Directionality*	This study
PLLA-TMC	Channels W: 5, 10, 25, 50, 100 μm D: 0.5, 1.0, 2.5, 5.0 μm	$\theta < 10°$	75–80%[c]	Myoblasts	ImageJ (method not specified)	[29]
PC	Channels W: 10 μm D: 5.1 μm	$\theta < 10°$	48 ± 11%	Nuclei	Image pro software	[41]
PEG-RGD hydrogel	Channels W: 40, 100 and 200 μm D: 100 and 200 μm	$\theta < 15°$	89%[d]	Myoblasts	Manual alignment quantification	[45]
PLA nanofibers	Fibre diameters 485.25 ± 107.64 nm	$\theta < 10°$	c.a. 90%	Myotubes	Not specified	[46]

Abbreviations: D = depth. Decell. = decellularized. hDF = human dermal fibroblasts. PC = polycarbonate. PEG-RGD = poly(ethylene glycol) with RGD. PLA = polylactic acid. PLLA-TMC = poly-L-lactide/trimethylene carbonate. OA = orientation angle. TCP = tissue culture plastic. W = width.
[a]Dimensions not specified.
[b]Not applicable to alignment quantitation method.
[c]5 × 5 μm channels.
[d]40 × 200 μm channels.

referred to as channels) produced on biomaterials via techniques such as polymer casting, 3D printing, electron or optical focused beam lithography, interference lithography, photolithography, and etching.[29,34,35,41,43-45]

The applicability of decellularized grass as a scaffold for skeletal muscle tissue engineering was assessed through the *in vitro* culture of C2C12 cells. The results demonstrated that decellularized grass supported the culture of C2C12 cells without the need for functionalization or modification, as demonstrated by the attachment efficiency of 35% ± 7%, significantly greater than the 9% ± 7% for native grass (Figure 4(a)). This is suspected to be a result of removing the waxy cuticle and exposing the ECM of the decellularized grass. The relatively low attachment efficiency of 35% is likely to be the result of the seeding method, where grass blades were untethered in the well, settling on the bottom of the well due to their density, rather than being tethered in any way. Attachment relies on the probability of passive cell-to-grass contact and this would have been diminished by the untethered scaffold. Nonetheless, these scaffolds displayed a

significant level of inherent adhesion despite the lack of modification or optimization of the seeding conditions.

Cell proliferation is presented in Figure 4(b), quantitatively demonstrating exponential cell growth up to confluence, which was reached between 4 and 6 days post-seeding. The growth rate of C2C12 cells on decellularized grass (doubling time of 25.7 hr between day 1 and 3 post-seeding) was comparable with *in vitro* scaffold-based studies in the literature, such as, 24.6 hr on aligned, electrospun PLA nanofibers[46] and ~24 to 34 hr on RGD-functionalized alginate of varying M:G ratio.[47] However, as expected, growth was slower than on TCP (19.7 ± 0.5 hr).[48]

A high cell viability of ~95% over a 7 day proliferation period was demonstrated as another measure of cytocompatibility, indicating that the scaffold is non-cytotoxic in accordance with the ISO standard requirements of viability >70%.[49] This is also comparable with other *in vitro* studies on decellularized scaffolds such as 98 ± 1% for C2C12 cells on decellularized apple slices after 12 weeks and >95% for cardiac cells on a decellularized heart after 8 days.[7,9]

Hence, decellularized grass was able to support the adhesion and proliferation of a highly-viable population of C2C12 myoblasts without the need to functionalize the scaffold following the decellularization process, unlike a number of decellularized plant studies which involved treatments such as RGDOPA functionalization, biomineralization, fibronectin coating, crosslinking with glutaraldehyde or modifying surface charge to improve cell attachment on cellulose-based scaffolds.[8,9,13,20] In some cases, such as the apple derived scaffolds used by Modulevsky et al, C2C12 cells were found to proliferate well in both unmodified and modified scaffolds.[9]

Previous studies have shown that materials with patterned topography in both the nano- and micrometre scale can influence cell behaviour, and that grooved surfaces (also referred to as grating, channels, ridges, steps and cliffs) support cell alignment along the axis of the grooves.[34,35] The use of decellularized plant tissue, specifically grass as a nano- and micropatterned scaffold, presents the advantages of being significantly cheaper and more readily accessible or available than typical micropattern fabrication techniques, which can be time-consuming, expensive and require access to intricate equipment.[34]

The natural topography of decellularized grass was shown here to support the self-alignment of cells via contact guidance with features in both the nano- and micro-scale, demonstrated by the images and preferred orientation plot in Figure 6. Alignment of C2C12 myoblasts was quantified to evaluate the effect of decellularized grass topographic features on inducing contact guidance driven cell behaviour. Compared to the random orientation of cells on the control of TCP (14% ± 2% within $\theta < \pm 10°$), cell alignment was clearly seen on decellularized grass (43% ± 8% within $\theta < \pm 10°$) as quantified via the *Directionality* plug-in for ImageJ, satisfying the hypothesis of this study.

Qualitatively, the alignment visualized using images of stained live cells (Figures 4(c) and 6) suggested that the cells were more aligned than suggested by the *Directionality* plug-in analysis. To further investigate C2C12 cell alignment, analysis of stained nuclei was undertaken using CellProfiler™ to quantify their orientation angle and the results obtained indicated a greater proportion of aligned cells. The alignment results in this study for cells aligned within $\theta < \pm 20°$ were 59% ± 8% using the *Directionality* plug-in for ImageJ and 72% ± 1% using CellProfiler™ for nuclei orientation. This suggests that different methods of quantifying alignment result in perceived differences of the degree of alignment and, consequently, direct comparisons between studies may not be possible. Nonetheless, the results reported in this study compare very favourably with previous alignment studies in the literature. A comparison of cell alignments on different substrates is provided in Table 1, highlighting the reported topographic dimensions, alignment basis and quantification methods. It is clear that grass blades offer superior cell alignment compared to other decellularized plant scaffolds, namely *Solenostemon* stems and parsley stems. Although using human dermal fibroblasts rather than myoblasts Fontana et al. demonstrated that by measuring nuclear orientation, 44.1% ± 7.2% and 28.6 ± 3.4% of cells on *Solenostemon* stems and parsley, respectively, were observed to align within $\theta < \pm 20°$ of the grooves of the scaffolds.[13] In this study, using the same methodology to determine alignment, 72% ± 1% of cells were within $\theta < \pm 20°$ and

53% ± 4% were within $\theta < \pm 10°$, clearly demonstrating that the microstructures within decellularized grass scaffolds were extremely effective at promoting aligned cell growth. The extent of cell alignment reported here is not as pronounced, however, as that observed in the majority of studies where C2C12 cells were grown on synthetic scaffolds fabricated to possess topographical cues (Table 1). With the exception of a study by Charest et al., where 48 ± 11% of myoblasts aligned within $\theta < \pm 10°$ on grooved polycarbonate, these studies achieved 75–90% alignment of cells within $\theta < \pm 10°$ or ± 15°, although methods for quantifying cell alignment varied.[29,41,45,46] By their nature, the methods used to generate synthetic scaffolds with topographical cues are less prone to variation than the structures found within natural scaffolds (Figures S1, S3, 2 and 3), but they can involve considerable expense, time and technical expertise. Decellularized grass scaffolds achieved over 50% cell alignment within $\theta < \pm 10°$ and over 70% within $\theta < \pm 20°$ via contact guidance (Figures 4(c), 5 and 6), which is more than sufficient for many anisotropic tissue engineering applications, and they can be generated with very little investment of time or resources, and without the need for further modification or processing. Interestingly, the optimum channel dimensions in many studies of C2C12 alignment, at the lower end of micro-scale, are analogous to the feature sizes found to be present on decellularized grass (Table 1). It is also worth noting for future applications in skeletal muscle tissue engineering that primary myoblasts reportedly exhibit improved alignment on a given scaffold in comparison to C2C12 myoblasts.[41]

With the goal of engineering skeletal muscle, differentiation of mononuclear cells into multinuclear myotubes is required. Importantly, the fact that decellularized grass is shown to support the alignment of C2C12 myoblasts in a preferred orientation, parallel to the axis of the grass blade, satisfies the prerequisite for passive differentiation into aligned myotubes.[29,30] This was confirmed with C2C12 myoblasts, which fused together on decellularized grass blades to form aligned multinuclear myotubes with lengths of >400 μm (Figure 7), replicating the anisotropic nature of skeletal muscle. While C2C12 cells, being murine myoblasts, are not the intended cells for the generation of engineered skeletal muscle tissue for regenerative medicine or cultured meat, this work presents a model scaffold with applicable features for the culture of skeletal muscle cells for these eventual applications. Cell alignment as a desired feature for tissue engineering, is not solely applicable to skeletal muscle tissue engineering; multiple reviews summarize studies used to guide alignment of endothelial cells, smooth muscle cells, fibroblasts, epithelial cells, corneal endothelial cells, neuroblastoma cells and mesenchymal stem cells directed to neuronal lineages.[33,34,37] Due to the mechanism of contact guidance, the natural topography of decellularized grass has the potential to be applicable to multiple tissue targets for passive alignment via topographic cues.

5 | CONCLUSIONS

Here, we have demonstrated the novel concept of using decellularized, garden-variety grass as a potential scaffold for skeletal muscle tissue

engineering. The results obtained reveal the successful decellularization of grass and its subsequent use as a scaffold that supports the attachment, maintenance of viability, proliferation, and differentiation of C2C12 cells. The attachment results indicate C2C12 cells preferentially adhere to grass that has been decellularized over native grass. Topography analysis of grass illustrates how the natural striations, visible by the naked eye, are channel-like, running parallel to the length of grass blades with depth variation in both the nano- and micro-scale. The channelled topography is subject to natural variation and non-homogeneity but supports the uniaxial self-alignment of C2C12 cells in their myoblast state via contact guidance, a feature retained following differentiation into myotubes. This presents advantages for future skeletal muscle tissue engineering applications as an inexpensive, readily available, preformed scaffold architecture with potential application as a passive means of culturing anisotropic muscle tissue *in vitro* without the need for additional manipulation to induce cellular alignment.

CONFLICT OF INTEREST

Scott Allan and Paul De Bank have no conflicts of interest. Marianne Ellis is co-founder of Cellular Agriculture Ltd.

DATA AVAILABILITY STATEMENT

The raw and processed quantitative data required to reproduce these findings are available to download from http://dx.doi.org/10.17632/5mgnz3zrmv.1

ORCID

Marianne J. Ellis https://orcid.org/0000-0003-4155-0853
Paul A. De Bank https://orcid.org/0000-0002-5717-7486

REFERENCES

1. O'Brien FJ. Biomaterials & scaffolds for tissue engineering. *Mater Today*. 2011;14:88-95.
2. Agrawal CM, Ong JL, Appleford MR, Mani G. *Introduction to biomaterials: basic theory with engineering applications*. New York, NY: Cambridge University Press; 2013.
3. Campuzano S, Pelling AE. Scaffolds for 3D cell culture and cellular agriculture applications derived from non-animal sources. *Front Sustainable Food Syst*. 2019;3:38.
4. Gilpin A, Yang Y. Decellularization strategies for regenerative medicine: from processing techniques to applications. *Biomed Res Int*. 2017;2017:9831534.
5. Badylak SF, Taylor D, Uygun K. Whole organ tissue engineering: decellularization and recellularization of three-dimensional matrix scaffolds. *Annu Rev Biomed Eng*. 2011;13:27-53.
6. Gilbert TW, Sellaro TL, Badylak SF. Decellularization of tissues and organs. *Biomaterials*. 2006;27:3675-3683.
7. Ott HC, Matthiesen TS, Goh S-K, et al. Perfusion-decellularized matrix: using nature's platform to engineer a bioartificial heart. *Nat Med*. 2008;14:213-221.
8. Gershlak JR, Hernandez S, Fontana G, et al. Crossing kingdoms: using decellularized plants as perfusable tissue engineering scaffolds. *Biomaterials*. 2017;125:13-22.
9. Modulevsky DJ, Lefebvre C, Haase K, Al-Rekabi Z, Pelling AE. Apple derived cellulose scaffolds for 3D mammalian cell culture. *PLoS One*. 2014;9:e97835.
10. Vogel J. Unique aspects of the grass cell wall. *Curr Opin Plant Biol*. 2008;11:301-307.
11. Crapo PM, Gilbert TW, Badylak SF. An overview of tissue and whole organ decellularization processes. *Biomaterials*. 2011;32:3233-3243.
12. Hodde J. Naturally occurring scaffolds for soft tissue repair and regeneration. *Tissue Eng*. 2002;8:295-308.
13. Fontana G, Gershlak J, Adamski M, et al. Biofunctionalized plants as diverse biomaterials for human cell culture. *Adv Healthc Mater*. 2017;6:1601225.
14. Cheng Y-W, Shiwarski DJ, Ball RL, Whitehead KA, Feinberg AWW. Engineering aligned skeletal muscle tissue using decellularized plant-derived scaffolds. *ACS Biomater Sci Eng*. 2020;6:3046-3054.
15. Lee J, Jung H, Park N, Park SH, Ju JH. Induced osteogenesis in plants decellularized scaffolds. *Sci Rep*. 2019;9:20194.
16. Campuzano S, Mogilever NB, Pelling AE. Decellularized plant-based scaffolds for guided alignment of myoblast cells. *BioRxiv*. 2020;958686.
17. Jones JD, Rebello AS, Gaudette GR. Decellularized spinach: an edible scaffold for laboratory-grown meat. *Food Biosci*. 2021;41:100986.
18. Klemm D, Heublein B, Fink HP, Bohn A. Cellulose: fascinating biopolymer and sustainable raw material. *Angew Chem Int Ed*. 2005;44:3358-3393.
19. Hickey RJ, Pelling AE. Cellulose biomaterials for tissue engineering. *Front Bioeng Biotechnol*. 2019;7:45.
20. Courtenay JC, Johns MA, Galembeck F, et al. Surface modified cellulose scaffolds for tissue engineering. *Cellulose*. 2017;24:253-267.
21. Courtenay JC, Deneke C, Lanzoni EM, et al. Modulating cell response on cellulose surfaces; tunable attachment and scaffold mechanics. *Cellulose*. 2018;25:925-940.
22. Domingues RMA, Gomes ME, Reis RL. The potential of cellulose nanocrystals in tissue engineering strategies. *Biomacromolecules*. 2014;15:2327-2346.
23. Dugan JM, Collins RF, Gough JE, Eichhorn SJ. Oriented surfaces of adsorbed cellulose nanowhiskers promote skeletal muscle myogenesis. *Acta Biomater*. 2013;9:4707-4715.
24. Ostrovidov S, Hosseini V, Ahadian S, et al. Skeletal muscle tissue engineering: methods to form skeletal myotubes and their applications. *Tissue Eng, Part B*. 2014;20:403-436.
25. Klumpp D, Horch RE, Kneser U, Beier JP. Engineering skeletal muscle tissue - new perspectives in vitro and in vivo. *J Cell Mol Med*. 2010;14:2622-2629.
26. Vandenburgh H. High-content drug screening with engineered musculoskeletal tissues. *Tissue Eng, Part B*. 2010;16:55-64.
27. Dunn A, Talovic M, Patel K, Patel A, Marcinczyk M, Garg K. Biomaterial and stem cell-based strategies for skeletal muscle regeneration. *J Orthop Res*. 2019;37:1246-1262.
28. Ben-Arye T, Levenberg S. Tissue engineering for clean meat production. *Front Sustainable Food Syst*. 2019;3:46.
29. Altomare L, Gadegaard N, Visai L, Tanzi MC, Farè S. Biodegradable microgrooved polymeric surfaces obtained by photolithography for skeletal muscle cell orientation and myotube development. *Acta Biomater*. 2010;6:1948-1957.
30. Lam MT, Huang YC, Birla RK, Takayama S. Microfeature guided skeletal muscle tissue engineering for highly organized 3-dimensional free-standing constructs. *Biomaterials*. 2009;30:1150-1155.

31. Jana S, Levengood SKL, Zhang M. Anisotropic materials for skeletal muscle tissue engineering. *Adv Mater*. 2016;28:10588-10612.

32. Engler AJ, Griffin MA, Sen S, Bönnemann CG, Sweeney HL, Discher DE. Myotubes differentiate optimally on substrates with tissue-like stiffness: pathological implications for soft or stiff microenvironments. *J Cell Biol*. 2004;166:877-887.

33. Tamiello C, Buskermolen ABC, Baaijens FPT, Broers JLV, Bouten CVC. Heading in the right direction: understanding cellular orientation responses to complex biophysical environments. *Cell Mol Bioeng*. 2016;9:12-37.

34. Bettinger CJ, Langer R, Borenstein JT. Engineering substrate topography at the micro- and nanoscale to control cell function. *Angew Chem Int Ed*. 2009;48:5406-5415.

35. Wilkinson CDW, Riehle M, Wood M, Gallagher J, Curtis ASG. The use of materials patterned on a nano- and micro-metric scale in cellular engineering. *Mater Sci Eng C*. 2002;19:263-269.

36. Wolf K, Müller R, Borgmann S, Bröcker E-B, Friedl P. Amoeboid shape change and contact guidance: T-lymphocyte crawling through fibrillar collagen is independent of matrix remodeling by MMPs and other proteases. *Blood*. 2003;102:3262-3269.

37. Flemming RG, Murphy CJ, Abrams GA, Goodman SL, Nealey PF. Effects of synthetic micro- and nano-structured surfaces on cell behavior. *Biomaterials*. 1999;20:573-588.

38. Lam MT, Sim S, Zhu X, Takayama S. The effect of continuous wavy micropatterns on silicone substrates on the alignment of skeletal muscle myoblasts and myotubes. *Biomaterials*. 2006;27:4340-4347.

39. Schindelin J, Arganda-Carreras I, Frise E, et al. Fiji: an open-source platform for biological-image analysis. *Nat Methods*. 2012;9:676-682.

40. McQuin C, Goodman A, Chernyshev V, et al. CellProfiler 3.0: next-generation image processing for biology. *PLoS Biol*. 2018;16:e2005970.

41. Charest JL, García AJ, King WP. Myoblast alignment and differentiation on cell culture substrates with microscale topography and model chemistries. *Biomaterials*. 2007;28:2202-2210.

42. Adamski M, Fontana G, Gershlak JR, Gaudette GR, Le HD, Murphy WL. Two methods for Decellularization of plant tissues for tissue engineering applications. *J Vis Exp*. 2018;135:e57586.

43. Cha SH, Lee HJ, Koh WG. Study of myoblast differentiation using multi-dimensional scaffolds consisting of nano and micropatterns. *Biomater Res*. 2017;21(1):1-9.

44. Sun Y, Duffy R, Lee A, Feinberg AW. Optimizing the structure and contractility of engineered skeletal muscle thin films. *Acta Biomater*. 2013;9:7885-7894.

45. Hume SL, Hoyt SM, Walker JS, et al. Alignment of multi-layered muscle cells within three-dimensional hydrogel macrochannels. *Acta Biomater*. 2012;8:2193-2202.

46. Luo B, Tian L, Chen N, Ramakrishna S, Thakor N, Yang IH. Electrospun nanofibers facilitate better alignment, differentiation, and long-term culture in an: in vitro model of the neuromuscular junction (NMJ). *Biomater Sci*. 2018;6:3262-3272.

47. Rowley JA, Mooney DJ. Alginate type and RGD density control myoblast phenotype. *J Biomed Mater Res*. 2002;60:217-223.

48. Cheng CS, El-Abd Y, Bui K, et al. Conditions that promote primary human skeletal myoblast culture and muscle differentiation in vitro. *Am J Physiol Cell Physiol*. 2014;306:C385-C395.

49. International Organization for Standardization. ISO 10993-5:2009 (E) biological evaluation of medical devices. Part 5: tests for in vitro cytotoxicity. Geneva, Switzerland; 2009.

SUPPORTING INFORMATION

Additional supporting information may be found online in the Supporting Information section at the end of this article.